Measurement of F_2 and $R = \sigma_L/\sigma_T$ on Nuclear-Targets in the Nucleon Resonance Region (F2-Rnuclear-Hall-C)

Re-submission of P03-110 (deferred with regret by PAC24). First Stage of a Program to Investigate Quark Hadron Duality in Electron and Neutrino Scattering on Nucleons and Nuclei in Collaboration with the Fermilab MINERvA Experiment

A. Bodek (co-spokesperson), S. Manly, K. McFarland, I. Park (J. Chovjka, G.B. Yu),* (D. Koltun, L. Orr, S. Rajeev) †
Department of Physics and Astronomy, University of Rochester, Rochester, NY 14627

M.E. Christy, W. Hinton, (C. Jayalath)*, C. Keppel (co-spokesperson), E. Segbefia
Hampton University, Hampton, VA

P. Bosted, S. E. Rock
University of Massachusetts, Amherst, MA

G. Niculescu, I. Niculescu
James Madison University, Harrisonburg, VA

R. Ent, D. Gaskell, M. Jones, D. Mack, S. Wood
Thomas Jefferson National Accelerator Facility, Newport News, VA

J. Arrington
Argonne National Laboratory, Argonne, IL

H. Gallagher
Tufts University, Medford, MA

J. Dunne
Mississippi State University, Mississippi State, MS

P. Markowitz, J. Reinhold
Florida International University, University Park, FL

E. Kinney
University of Colorado, Boulder, Colorado

H.P. Blok
Vrije Universiteit, Amsterdam, Netherlands

In collaboration with
The MINERvA Neutrino Experiment at Fermilab

---

*PhD thesis students, pending funding
†Collaborating theorists

I. SUMMARY

We propose to measure the longitudinal-transverse (L-T) separated structure functions F_2 and $R = \sigma_L/\sigma_T$ from nuclear targets in the resonance region. This re-submission of P03-110 (deferred with regret by PAC24) is the first stage of an overall program to investigate quark-hadron duality and electromagnetic and weak structure of nucleons and nuclei [1,2]. The targets proposed include Carbon, Quartz, Aluminum, Calcium, Steel and Copper to compliment existing baseline data on Hydrogen and Deuterium. The targets proposed are (or closely resemble) nuclear targets commonly used in neutrino experiments such as the low statistics bubble chamber experiments on Hydrogen, Deuterium, Neon, and Argon and high statistics neutrino experiments on Scintillator (MINERvA, MiniBONNE, K2K and JPARC), Water (SuperK, JPARC), Steel (MINOS) and Argon (CNGS). In addition to performing studies of quark-hadron duality in electron scattering on nuclear targets for the separated structure functions, these data will used as input vector form factors in a future analysis of neutrino data in order to investigate quark hadron-duality in the axial structure function of nucleons and nuclei. This will be done in collaboration with the MINERvA neutrino experiment [2] to be run in the NUMI [3] low energy neutrino beam at Fermilab.

An immediate impact of these new measurements with nuclear targets will be the reduction in uncertainties in neutrino oscillation parameters for current and near term neutrino oscillations experiments such as K2K and MINOS. The data are even more important for the more precise next generation neutrino oscillations experiments such as JPARC and NUMI Off-axis.

Measurements will be made in the nucleon resonance region ($1 < W^2 < 4\,\text{GeV}^2$) spanning the four-momentum transfer range $0.5 < Q^2 < 4.0\,(\text{GeV/c})^2$ at identical kinematic points to those to be run during JLab Deuterium experiment 02-109. (Therefore, it is most efficient for both experiments to be run at the same time). The decomposition of the inclusive electroproduction cross sections into longitudinal and transverse strengths will accomplished by performing Rosenbluth separations to extract the transverse structure function $F_1(x, Q^2)$, the longitudinal structure function $F_L(x, Q^2)$, and the ratio $R = \sigma_L/\sigma_T$.

The analysis of the separated resonance region proton data from experiment E94-110 [4], which was performed in Hall C, has recently been completed and the excellent precision obtained from that measurement is presented here. The extension of the proton measurements to deuterium is approved and will be run by E02-109 [5]. This proposal (P03-110) represents the first global survey of these fundamental separated quantities in the resonance region for nucleons bound in nuclei. Data from all of the previous experiments will be incorporated into the analysis.

Given the experience of previous experiments, the data taking is straightforward and allows the precision of the proposed measurements to be predicted with great confidence. In addition, the analysis machinery which was developed for E94-110 can be used with only very little modification. The great care and time invested in developing the experimental requirements, systematic uncertainty measurements, and analysis machinery will be of immediate benefit to the proposed experiment. We will also build upon the experience from previous lower statistics studies with (electrons) of the nuclear-dependence of the separated structure functions in the DIS region that were done by SLAC experiment E140 [6], as well as the very low Q^2 high W^2 studies (to test the HERMES effect) that were done by JLab experiment E99-118 [7].
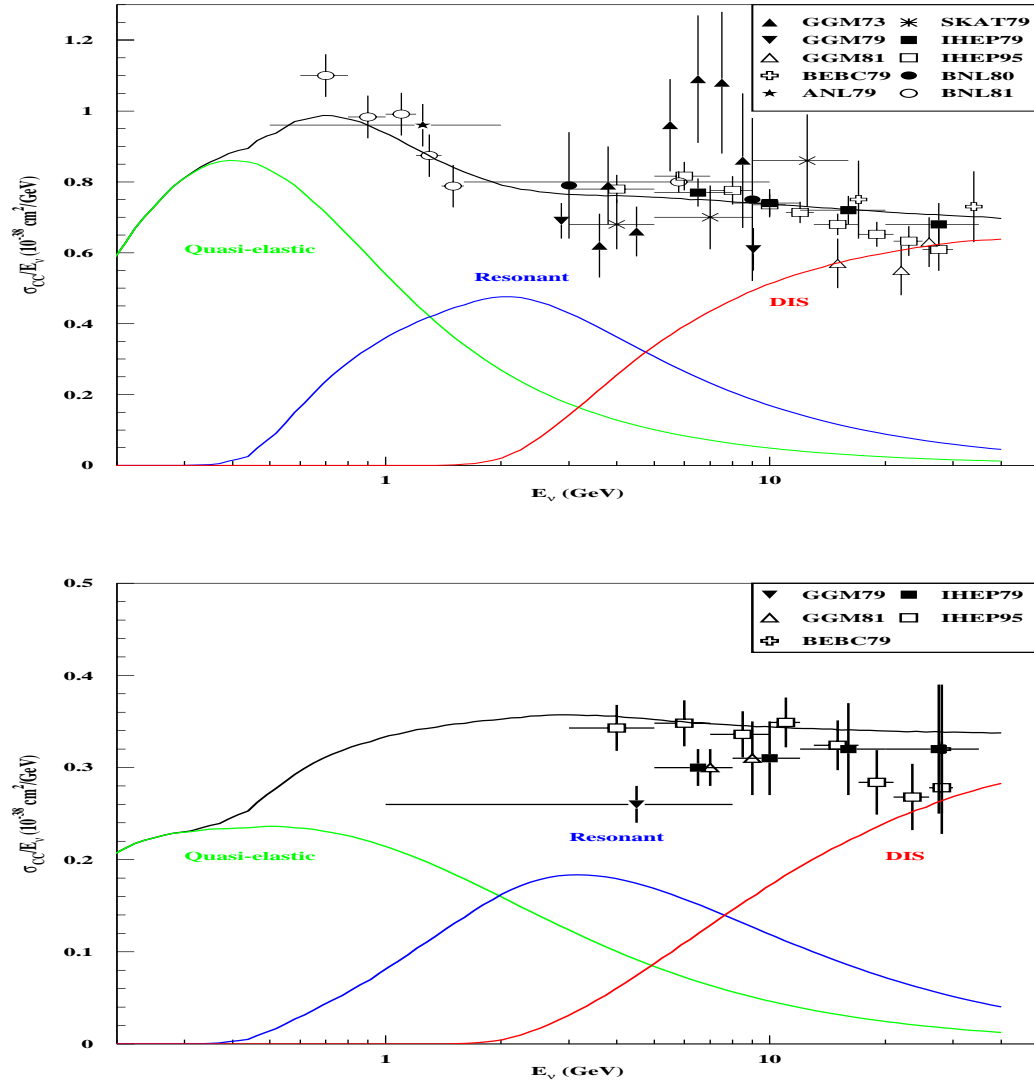
FIG. 1. Total neutrino and anti-neutrino cross-sections (*divided by energy*) versus energy compared to the sum of quasi-elastic, resonant, and inelastic contributions from the NUANCE model.

II. LOW-ENERGY ELECTRON AND NEUTRINO SCATTERING OVERVIEW

A. Form-Factors and Structure Functions

Several formalisms are used to discuss electron-nucleon and neutrino-nucleon scattering, and the corresponding reactions on nuclear targets.

Inclusive lepton scattering can be described in the language of structure functions or in terms of form-factors for the production of resonant final states. The two descriptions are equivalent and there are expressions relating form-factors to structure functions. In electron scattering, the vector form-factors can be related to the two structure functions W_1 and W_2 (which are different for neutrons and protons), or equivalently F_2 and R.

In neutrino scattering, there are three structure functions W_1, W_2 and W_3 (or F_2, R and xF_3), different for neutrons and protons, and containing both vector and axial-vector com-

ponents. There are also two other structure functions (important only at very low energies) whose contributions depend on the final-state lepton mass; these can be related to the dominant structure functions within the framework of theoretical models.

B. Electron versus Neutrino Scattering

From the conservation of the vector current (CVC), the vector structure functions (or form-factors) measured in electron scattering can be related to their counterparts in neutrino scattering for specific isospin final states. For elastic scattering from spin-$\frac{1}{2}$ quarks or nucleons, these relationships between vector form-factors are simple. For production of higher spin resonances, the relations are more complicated and involve Clebsch-Gordon coefficients.

In contrast, the axial structure functions in neutrino scattering cannot be related to those from electron scattering, except in certain limiting cases (for example, within the quark/parton model at high energies with V=A). At low Q^2, the axial and vector form-factors are different, e.g. because of the different interactions with the pion cloud around the nucleon.

Another difference arises from nuclear effects in inclusive neutrino vs. electron scattering. Nuclear effects on the axial and vector components of the cross-section can differ due to shadowing, and can also affect valence and sea quarks differently.

C. Sum Rules and Constraints

Several theoretical constraints and sum rules can be tested in electron and neutrino reactions (or applied in the analysis of data). Some of the sum rules and constraints are valid at all values of Q^2, and some are valid only in certain limits.

The Adler [24] sum rules apply separately to the axial and vector parts of W_1, W_2, and W_3 and are valid for all values of Q^2 (since they are based on current algebra considerations). At high Q^2, these sum rules are equivalent to the statement that the number of u valence quarks in the proton minus the number of d valence quarks is equal to 1.

Other sum rules, such as the momentum sum rule (sum of the momentum carried by quarks and gluons is 1) and the Gross/Llewelyn-Smith sum rule (number of valence quarks is equal to 3), have QCD corrections and break down at very low Q^2.

At very low Q^2, vector structure functions are constrained by the photoproduction cross-section. At high Q^2 it is expected that the structure functions are described by QCD and satisfy QCD sum rules.

D. Final States

Quasi-elastic[1] reactions, resonance production, and deep-inelastic scattering are all important components of neutrino scattering at low energies.

---

[1]We should clarify that the neutrino community uses the term 'quasi-elastic' to describe a charged-current process in which a neutrino interacts with a nucleon to produce a charged lepton in the final state. The nucleon can be a free nucleon or a nucleon bound in the nucleus. The term 'quasi-elastic' refers to the fact that the initial state neutrino changes into a different lepton, and there is a single recoil nucleon in the final state (which changes its charge state). In contrast, the electron scattering community refers to electron-nucleon scattering with a single recoil nucleon as 'elastic' scattering. The term 'quasi-elastic' scattering is used by the electron scattering community to describe elastic electron-nucleon scattering from bound nucleons in a nucleus. Here the term 'quasi-elastic' refers to the fact that the bound nucleon is quasi-free. Both nomenclatures are used in the literature.

To describe specific final states, one can use the language of structure functions, combined with fragmentation functions, at high values of Q^2. At low values of Q^2, many experiments describe the cross-sections for specific exclusive final states. Both of these pictures need to be modified when the scattering takes place on a complex nucleus.

E. Current status of Neutrino Cross Sections

Figure 1 shows the current data for total neutrino and antineutrino cross-sections *divided by energy* (per nucleon for an isoscalar target) versus energy (at low energies) compared to a model of the sum of quasi-elastic, resonant, and inelastic contributions. The current data has large uncertainties (from poor statistics and 20% errors in the neutrino flux).

Since all current models for the various components of the total neutrino cross section are not totaly consistent with each other, the predicted sum is constructed to be continuous in W as follows. For $W > 2$ GeV the Bodek-Yang model is used (with the axial structure functions calculated [28] with $Z = 0.5$). The Rein-Sehgal model is used used for $W < 2$ GeV. In addition, a fraction of the Bodek-Yang cross-section is added to the Rein-Sehgal cross-section between $W = 1.7$ GeV and $W = 2$ GeV. The fraction increases linearly with W from 0 to 0.38 between $W = 1.7$ and $W = 2$ GeV. These two figures also show the various contributions to the neutrino and antineutrino total cross-sections that will be investigated in the next generation high statistics low energy neutrino experiment such as MINERvA.

Quasi-elastic scattering and resonance production, either with neutrinos or with antineutrinos, provides the largest contributions to the total νN event rate in the threshold regime $E_\nu \leq 3$ GeV. This is the region of interest for current and next generation neutrino oscillations experiments.

For this reason, precise knowledge of the quasielastic and resonance production cross sections, including the energy dependence and its variation with target nuclei, is important to continued progress in current and future neutrino oscillation experiments. The poor knowledge of the neutrino total cross (divided by energy) shown in Figure 1 is similar to the current state of knowledge of the quasielastic reaction cross section. This is indicated by the compilations of previous experimental measurements of quasielastic cross sections with neutrino and antineutrino beams on various nuclear targets as shown in Figures 2 and 3. Among the results shown there are normalization uncertainties originating with flux uncertainties which are typically 10-20%. It is readily seen in these plots that existing measurements have large errors throughout the E_ν range accessible with the next generation neutrino experiments such as MINERvA (Fig. 2, upper plot), and especially in the threshold regime which is crucial to future neutrino oscillation experiments (Fig. 2, lower plot). Figure 3 shows this problematic lack of precision to pervade the anti-neutrino quasi-elastic cross section measurements as well.

The state of knowledge of resonance production in neutrino beams is even worse. Therefore, current neutrino oscillations experiment use theoretical models which rely heavily on input from electron scattering data on nucleons and nuclei for the vector contribution to all three contributions (quasielastic, resonance and deep inelastic) to the total neutrino cross sections and final states. The axial contribution is now estimated using models which are fit to low statistics neutrino data. This is expected to continue to be the case over the next five years.

F. Use in Neutrino Oscillations Experiments

Current neutrino oscillations experiments compare the measured neutrino cross section in a far detector to the expected cross section as a function of neutrino energy. A 10% dip in the cross section as a function of energy is interpreted as a disappearance of neutrinos originating from oscillations of neutrinos from one flavor to another (e.g. τ neutrinos which are below threshold). The amplitude of the dip gives the mixing angle, and the location of the dip in neutrino energy gives the difference in mass between the neutrino eigenstates. The uncertainty in the magnitude

of the disappearance originates from the uncertainty in the various contributions to the neutrino cross section as a function of neutrino energy in the energy region between 0.5 and 5 GeV.

The uncertainty in the location of the dip originates from uncertainties in the composition of the final states hadrons. The response of neutrino detectors to quasielastic muons, recoil protons, charged pions and neutral pions are all different. Therefore, the total neutrino energy observed in a calorimetric detector depends on assumed composition of the final state as a function of neutrino energy.
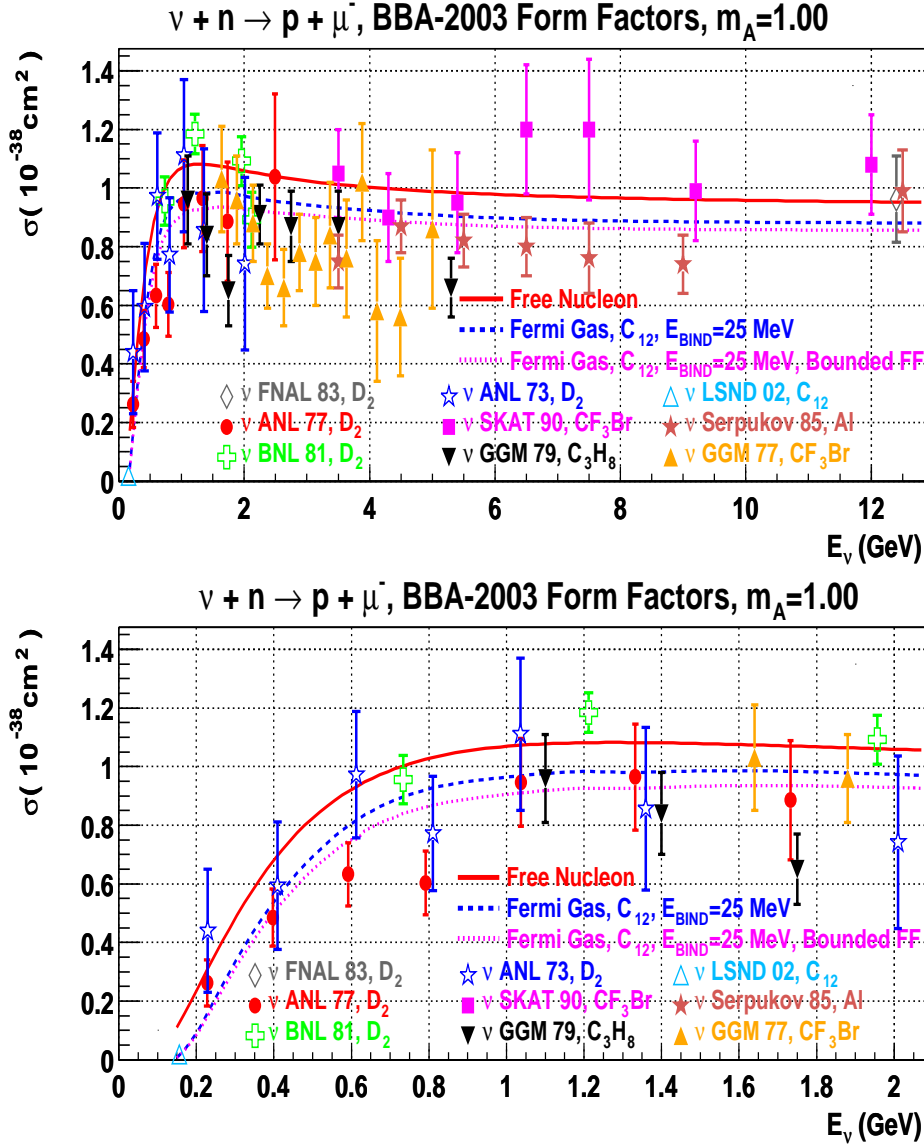

FIG. 2. Compilation of experimental measurements of the neutrino quasi-elastic cross section. Existing measurements are characterized by large errors throughout the E_ν range accessible to MINERνA (upper plot), especially so in the crucial threshold regime (lower plot). Representative calculations are shown using BBA-2003 form factors with M_A=1.00 GeV. The solid curve is without nuclear corrections, the dashed curve includes a Fermi gas model and the dotted curve includes Pauli blocking and nuclear binding. The data shown are from FNAL 1983 , ANL 1977 ,BNL 1981 , ANL 1973 , SKAT 1990 , GGM 1979 ,LSND 2002 , Serpukov 1985 , and GGM 1977

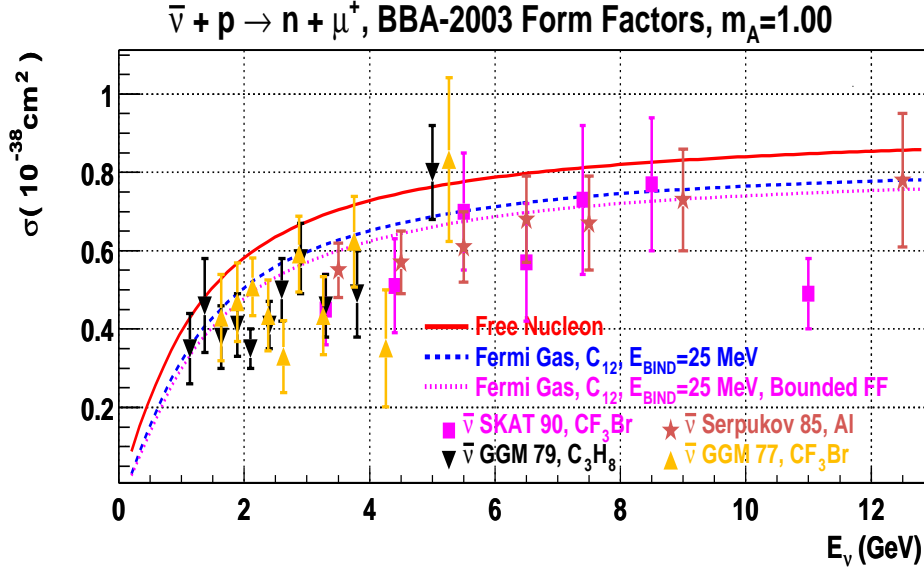**$\bar{\nu} + p \rightarrow n + \mu^+$, BBA-2003 Form Factors, m_A=1.00**

FIG. 3. Experimental measurements of the anti-neutrino quasi-elastic cross section over the energy range accessible to MINERvA. As with the neutrino quasi-elastic cross section results of Fig. 2, there is large dispersion among the among the anti-neutrino measurements including systematic differences between individual experiments. Theoretical expectations without (solid curve) and including nuclear corrections (dashed, dotted curves) are shown for comparison. The data shown are from SKAT 1990 , GGM 1979 , Serpukov 1985 , and GGM 1977 .

Therefore, in addition to these proposed measurements of inclusive structure functions on nuclear targets, the composition of various hadronic final states in electron scattering on Carbon will be also investigated in parallel effort by members of this collaboration. This effort is lead by Professor Steve Manly from Rochester and Dr. Will Brooks from Jlab, who plan to investigate final states using existing Hall B data on Carbon in a similar energy range.

G. Neutrino Near Detectors

Given the large investment in the next generation neutrino oscillations experiment (e.g. \$2B for JPARC and 250M for NUMI), neutrino oscillations experiments are taking a multiprong approach towards predicting the expected event rates in far detectors.

1. Reduce the error in the predicted neutrino flux by initiating new hadron production experiments to precisely measure the yield of pions and kaons (which decay to neutrinos). These are expected to provide a knowledge of the neutrino flux to a level of 1% to 2%.

2. The electron and neutrino scattering communities are collaborating in an experimental and theoretical program to measure and model lepton vector and axial scattering on nucleons and nuclei. The International Workshops on Neutrino-Nucleus Interactions in the Few GeV Region (NUINT [27]) were started in 2001 to communicate progress in this field.

3. New electron scattering experiments are being initiated to investigate inclusive and exclusive processes on nucleon and nuclear targets.

4. Fully active near detector neutrino experiments (such as MINERvA) are being initiated to investigate neutrino reactions in detail.

5. Small replicas of the neutrino far detectors (which are not fully active and are constructed of nuclear targets) are used as additional near detectors. In principle, neutrino flux, cross sections and nuclear effects cancel in a comparison of rates between this kinds of near

detector and the far detectors. However, because of solid angle effects, the neutrino flux in these replica near detectors is different from the neutrino flux in the far detector, so the flux effects do not completely cancel. In addition, because the two detectors are of such vastly different size, detector effects do not completely cancel either.

It is generally agreed that all of the above approaches are needed for the next generation round of experiments.

III. PHYSICS OVERVIEW, MOTIVATION AND GOALS

As is described in the following sections, the physics emphasis of the next generation neutrino experiments at low energy such as MINERvA is two fold. (a) First, the investigation of neutrino cross sections and final states at low energies as a tool to study neutrino oscillations, and (b) a complete investigation of vector and axial structure functions and form factors on nucleons and nuclei, sum rules and quark-hadron duality. The second part is expected to be an ongoing program culminating in the end of 2009 (when MINERvA is scheduled to complete its data taking). By the end of this decade, combined information from electron and neutrino scattering can be used to investigate the difference between vector and axial form factors and structure functions on nuclear targets with very high precision.

Members of this collaboration are proposing to investigate quark-hadron duality in high statistics electron scattering with the same nuclear targets first. This will be followed by a comparison the electron scattering data with all existing neutrino data, with the aim of continuing these studies in the future with the high statistics neutrino experiment in the the MINERvA experiment at the Fermilab NUMI low energy neutrino beam. The investigation of quark-hadron duality in both the axial structure functions of nucleons and nuclei with both electrons and neutrinos is complementary. *Separation of vector and axial-vector components in neutrino scattering is only possible if the vector part is provided from electron scattering experiments as described below.*

A. Kinematics

Due to the small value of the electromagnetic coupling constant, the scattering of electrons from nucleons can be well approximated by the exchange of a single virtual photon, which carries the exchanged 4-momentum squared, q^2. In terms of the incident electron energy, E, the scattered electron energy, $E^{'}$, and the scattering angle, θ, the absolute value of the exchanged 4-momentum squared is given by

$$(-q)^2 = Q^2 = 4EE^{'}\sin^2\frac{\theta}{2}. \tag{1}$$

In the one photon exchange approximation, the spin-independent cross section for inclusive electron-nucleon scattering can be expressed in terms of the photon helicity coupling as

$$\frac{d\sigma}{d\Omega dE'} = \Gamma\left[\sigma_T\left(x, Q^2\right) + \epsilon\sigma_L\left(x, Q^2\right)\right], \tag{2}$$

where σ_T (σ_L) is the cross section for photo-absorption of purely transverse (longitudinal) polarized photons,

$$\Gamma = \frac{\alpha E^{'}\left(W^2 - M_p^2\right)}{2\pi Q^2 M_p E\left(1 - \epsilon\right)} \tag{3}$$

is the flux of transverse virtual photons, and

$$\epsilon = \left[1 + 2(1 + \frac{\nu^2}{Q^2}) \tan^2 \frac{\theta}{2} \right]^{-1} \tag{4}$$

is the relative flux of longitudinally polarized virtual photons.

In terms of the structure functions $F_1(x, Q^2)$ and $F_L(x, Q^2)$, the double differential cross section can be written as

$$\frac{d\sigma}{d\Omega dE'} = \Gamma \frac{4\pi^2 \alpha}{x(W^2 - M_p^2)} \left[2x F_1(x, Q^2) + \epsilon F_L(x, Q^2) \right]. \tag{5}$$

Comparison of equations 2 and 5 shows that $F_1(x, Q^2)$ is purely transverse, while the combination

$$F_L(x, Q^2) = \frac{1 + 4M_p^2 x^2}{Q^2} F_2(x, Q^2) - 2x F_1(x, Q^2) \tag{6}$$

is purely longitudinal. The separation of the unpolarized structure functions into longitudinal and transverse parts from cross section measurements can be accomplished via the Rosenbluth technique [8], by making measurements at two or more values of ϵ for fixed x and Q^2. Fitting the reduced cross section, $d\sigma/\Gamma$, linearly in ϵ, yields σ_T (and therefore $F_1(x, Q^2)$) as the intercept, and the structure function ratio $R(x, Q^2) = \sigma_L/\sigma_T = F_L(x, Q^2)/2x F_1(x, Q^2)$ as the slope.

Further information on electron and neutrino structure functions is given in Appendix D.

As mentioned earlier, in neutrino scattering separating vector and axial structure functions is done by relating the neutrino vector structure functions to the separated vector structure functions in electron scattering on protons and neutrons via CVC and Clebsch-Gordan coefficients which depend on the contributions of different isospin amplitudes to the scattering. The relations between the vector structure functions are well determined for elastic (quasi-elastic) scattering on free nucleons for which the isospin of the initial and final states are well determined. Similarly, the relationships between the vector form factors are also well determined for the scattering on free quarks (i.e.the high Q^2 DIS scattering) for which the isospin states of the initial and final state quarks are also well determined. In general, even in these well understood cases, in order to extract the axial structure function in neutrino scattering experiments, the separated vector structure functions from electron scattering, F_{2p}, F_{2n}, R_p, R_n for bound nucleons are needed.

In the resonance region which includes contributions from final states with different isospins, the relationships between the vector form factors in neutrino and electron scattering is more complicated. Therefore, a unified investigation of quark-hadron duality for the same nuclear targets with electrons and neutrinos is interesting.

High statistics samples in neutrino experiments on nuclear targets such as iron and hydrocarbons will be measured beginning in 2005 in experiments at the near detector hall at the Fermilab-NUMI beam

A large unknown is the value of R in the resonance region for both vector and axial scattering on nuclear targets in the resonance region. In addition, the axial part of F_2 and $x F_3$ are not well known. The nuclear dependence of R in the resonance region at low Q^2 and W has not been measured in either vector or axial scattering. Figure 4 (left) shows the world's data on R for all nuclear targets in the DIS region. Figure 4 (right) shows all available data on the nuclear dependence of R in the DIS region. The errors are very large and none of the data are in the resonance region. Note that the data in Figure 4 (right) were taken at high values of W^2 in the DIS region. At these high W and Q^2 values, the overall value of R is generally quite small. Therefore, nuclear effects cannot be discerned by the these DIS data. The new measurements proposed here are at low Q^2, where R is larger and a nuclear dependence easier to discern. As discussed in following secxtions, theoretical models indicate that the largest nuclear dependence of R is expected to be in the resonance region at low Q^2 (see figure 8). The lines in Figure 4 (right) represent the small projected uncertainties of the new measurements proposed by here (P03-110).

Figures 7 and 6 show preliminary results of analysis of data from Jlab experiment E94-110 [4] on hydrogen in the resonance region. Data with deuterium is expected to be taken in experiment E02-109, and data with nuclear targets is proposed to be taken by this proposal (P03-110).
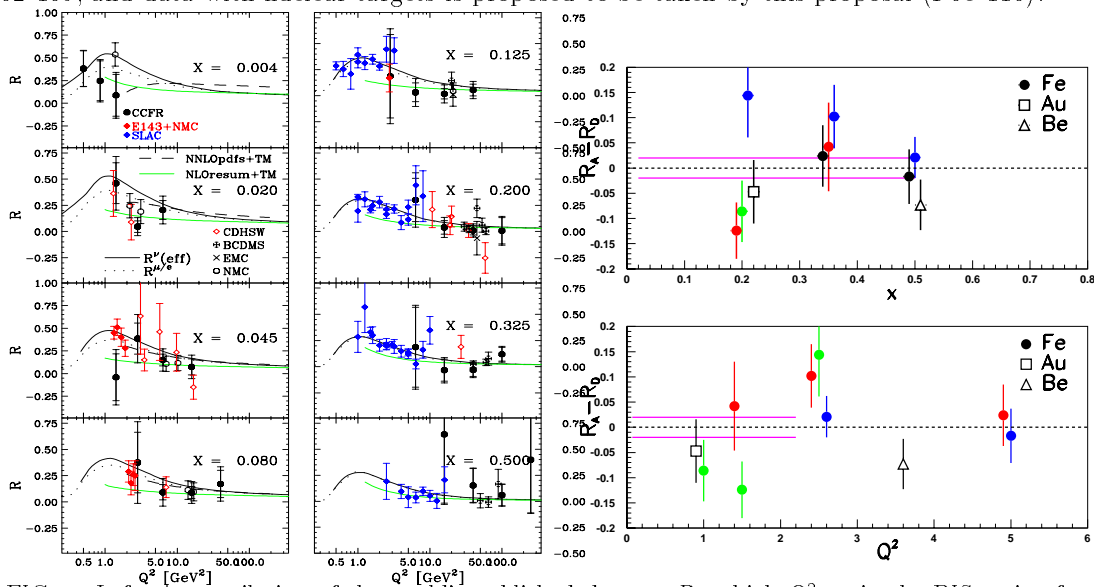

FIG. 4. Left: A compilation of the world's published data on R at high Q^2 on in the DIS region for both nucleons and nuclei. Right: The SLAC E140 data on the nuclear dependence of R in the DIS region presented in the form $R_A - R_D$ (e.g. difference between iron and deuterium. The lines in rhw figure on the right represent the small projected uncertainties of the new measurements proposed by here (P03-110).
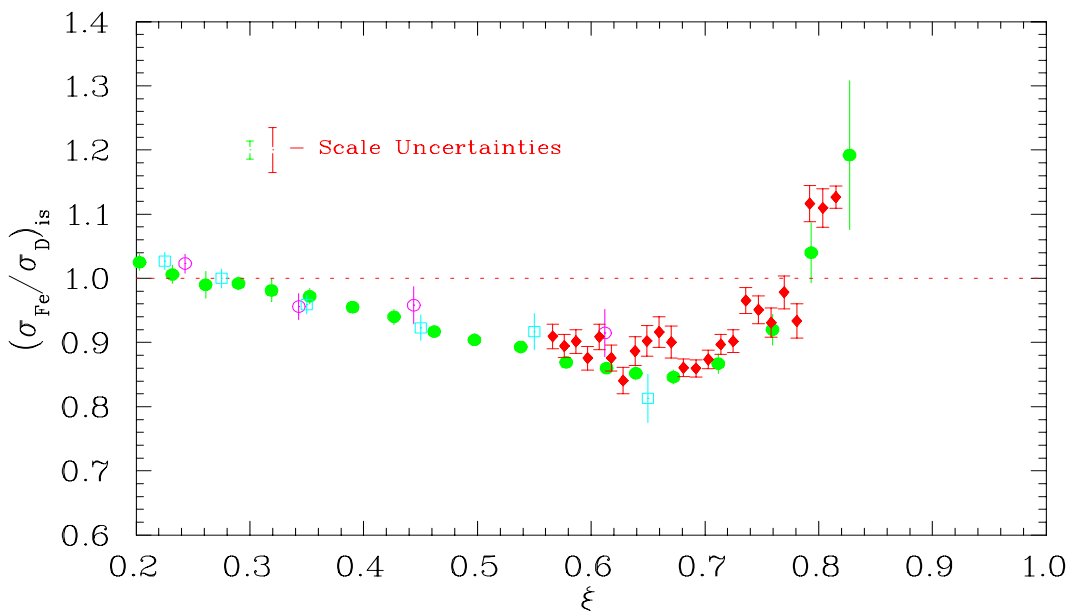

FIG. 5. A comparison of the ratio of cross sections of iron to deuterium in the resonance region versus the ratio measured in the DIS region. These preliminary data from JLab indicate that the nuclear effects in the DIS and resonance region are the same if plotted versus the Nachtman variable as expected from duality. Note that since these are ratios of cross sections and not of separated structure functions. Therefore, it is necessary to assume that there is no nuclear dependence of R in order to interpret these data.
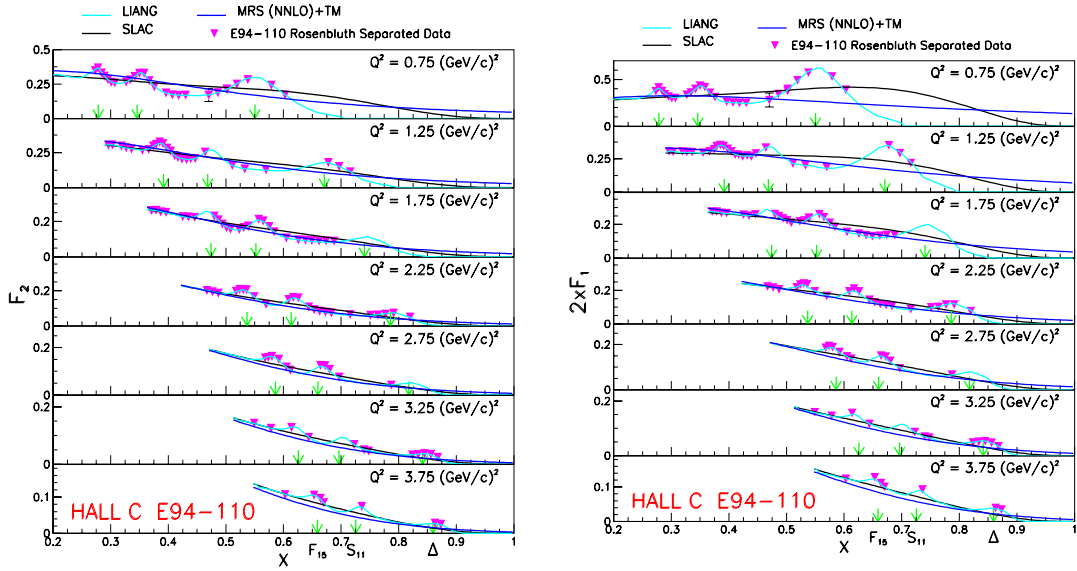
FIG. 6. Recent data from Jlab experiment E94-110 (on Hydrogen) for $2xF_1$ (left) and F_2 (right) in the resonance region. Data with deuterium is expected to be taken in experiment E02-109, and data with nuclear target is proposed to be taken by P03-110.

FIG. 7. Recent data from Jlab experiment E94-110 (on hydrogen) for R (left) and F_L (right) in the resonance region. Data with deuterium is expected to be taken in experiment E02-109, and data with nuclear target is proposed to be taken by P03-110.
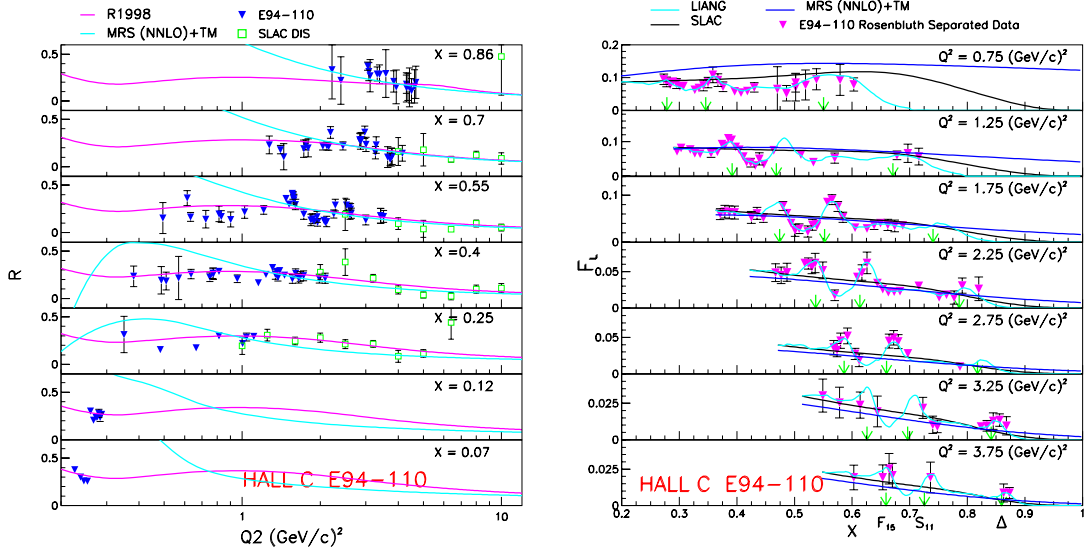
The R_{1998} function provides a good description of the world's data . However, at low Q^2 and low W the nuclear effects on R are not known.

The existing world's data measurements of the nuclear dependence of R in the DIS region from SLAC Experiment E140 [6] are shown in Figure 4 (right). As seen in the figure, the errors in the DIS region are very large, and no data exists in the resonance region. Preliminary JLab data on tests of duality for F_2 in the resonance region at higher Q^2 is shown in Figure 5. Note that since these are ratios of cross sections and not of separated structure functions. Therefore, it is necessary to assume that there is no nuclear dependence of R in order to interpret these data. At large Q^2 the nuclear effects in the resonance region are the same as in the DIS region for

the same value of the Nachtman scaling variable. At lower values of Q^2 duality in the Nachtman variable breaks down (as discussed in the next section), and the nuclear effects in F_2, $2xF_1$ and R could be very different.

IV. THE NUCLEAR DEPENDENCE OF R AND ITS RELATION TO NUCLEAR PHYSICS

A measurement of R in the region covered by this experiment also provides information about the dynamics of the internucleon force inside nuclei. For example, new calculations by Miller [29] predict a significant pion excess enhancement in the σ_L^A/σ_L^D ratio at low Q^2 and moderate x_Bj, as shown in figure 8. The kinematics of Miller's maximum pionic enhancement effects, which require a study of the A-dependence of the longitudinal cross section in the resonance region, fall within the proposed measurement. The question "Where are the nuclear pions?" has been an outstanding problem in nuclear physics for decades now. The belief that pions are the carrier of the nuclear force is a basic premise of nuclear physics, and yet is is not an experimentally verified one. While this premise *seemed* verified by the original electromagnetic scattering (EMC effect) experiments, it was later brought into question by deep inelastic Drell-Yan lepton-nucleus measurements. Further, no single theory of pionic nuclear binding has been able to reconcile all of the observations at all kinematics. As Miller concludes, the proposed new data will present "an excellent opportunity to unravel a significant long-standing mystery involving the absence of nuclear pionic effects."
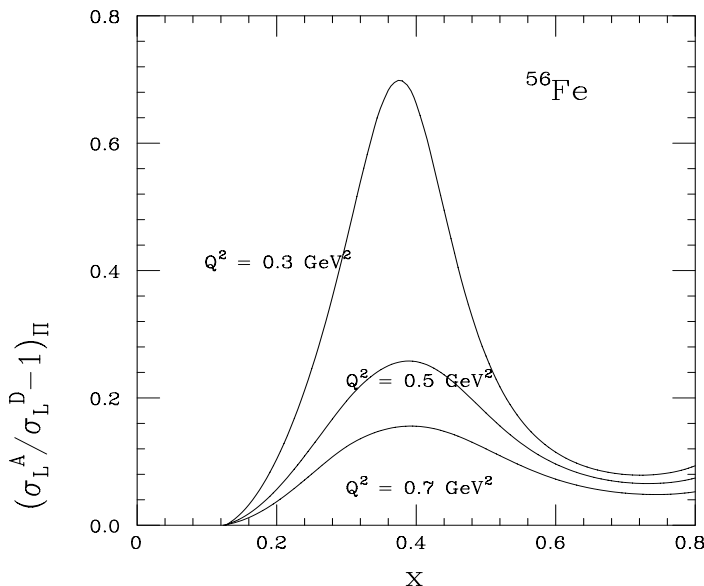
FIG. 8. Plot from G. A. Miller (Phys.Rev. C 64,022201(2001)) showing the predicted sensitivity of the inclusive longitudinal cross section ratio of Iron to Deuterium due to pion excess.

V. SENSITIVITY OF THE NEUTRINO CROSS SECTIONS TO R

The expressions used in this section are from Appendix D.

Within the quark-parton model, the total neutrino and antineutrino cross sections on a nucleon target are given by integrating the differential cross sections over x and y:

$$\sigma^{\nu N} = \frac{G_F^2 M E_\nu}{\pi(1 + Q^2/M_W^2)^2} \left[Q^{\nu N} + (1/3)\overline{Q}^{\nu N} + K^{\nu N} \right] \tag{7}$$

$$\sigma^{\overline{\nu} N} = \frac{G_F^2 M E_\nu}{\pi(1 + Q^2/M_W^2)^2} \left[\overline{Q}^{\overline{\nu} N} + (1/3)Q^{\overline{\nu} N} + K^{\overline{\nu} N} \right] \tag{8}$$

Here Q is the fractional momentum carried by all quarks in the nucleon, $\overline{Q}$ is the fractional momentum carried by all antiquarks in the nucleon and $R = 2\mathrm{K}/(Q+\overline{Q})$ is the average ratio of longitudinal to transverse contribution. For low energies, the antiquark contribution is small. Therefore, the fractional error in the predicted neutrino and antineutrino total cross sections from an uncertainty in R is $0.5\Delta R$ for neutrinos and $1.5\Delta R$ for antineutrinos, respectively.

In the region of the first resonance, R is predicted to be zero in the bound quark oscillator model. In fact, the first results from Jlab experiment E94-110 on hydrogen (shown in Figure 7) show a value of R of about 0.3 at low W and low Q^2. This implies that the effects of the nucleon pion cloud are very important in this region. The nuclear dependence of R in the region is totally unknown, and current measurements of the nuclear dependence of R have an error of ΔR of 0.2. It is expected that the nuclear effects on the nucleon pion cloud are very significant at low energies. Therefore, even if we use the preliminary precise measurement of R on hydrogen from experiment E94-110, we are still left with the problem that none of the data have been taken on Carbon or iron. An error ΔR of 0.2 implies a 10% error in the predicted neutrino cross section in this region and an error 30% in the predicted antineutrino cross setion.

A back of an envelope calculation of the sensitivity of the ratio of antineutrino to neutrino total cross section ratio to a change in the average value of R with neutrino energy or from nuclear effects (e.g. $R = 0.3 \pm 0.2$) is illustrative. At low energy, with $\overline{Q}$=0 we obtain the following. If $R = 0$, the ratio is 0.33. If $R = 0.5$, the ratio is $(0.33 + 0.25)/(1.0 + 0.25)$=0.46. The data shown in Figure 1 span all of this range.

Therefore, new measurements of the inclusive structure functions on nuclear targets with electrons this energy region can reduce the errors on the vector cross sections by a factor of 10. This can be done with about 5 days of running in Hall C, as described in the rest of this proposal.

VI. BROAD IMPACT OF THESE MEASUREMENTS ON NEUTRINO PHYSICS

A detailed study of F_2 and $R = \sigma_L/\sigma_T$ on nuclear targets in the resonance region is an important ingredient in forming an integrated description of charged lepton and neutrino scattering cross-sections. High rate neutrino beams now under construction or planned at Fermilab and J-PARC will allow the first precision experimental comparisons of electron and neutrino cross-sections and present and future neutrino oscillation experiments will use these results to predict event rates.

The recent discoveries of neutrino oscillations in atmospheric neutrinos [9] and in neutrinos from the sun [10,11] motivate the detailed studies of neutrino oscillations at future high intensity neutrino beams from accelerators. The two disparate mass scales observed in oscillations from these astrophysical sources, $\delta m^2{}_{\mathrm{atm}} \approx 2 \times 10^{-3}\mathrm{eV}^2$ and $\delta m^2{}_{\mathrm{solar}} \sim 10^{-4}\mathrm{eV}^2$, along with the stringent limits on $\overline{\nu}_e$ disappearance at the atmospheric L/E in the CHOOZ and Palo Verde reactor experiments experiments [13,14], have raised the possibility that there may be an observable CP-asymmetry in $\nu_\mu \to \nu_e$ transitions. This rare, sub-leading transition in the neutrino flavor sector is analogous to to searching for first and third generation mixing in the quark sector, which has led to a rich phenomenology of CP-violation, meson mixing and rare decays in the quark sector.

These neutrino oscillation experiments are very challenging, because of the required L/E of 400 km/GeV, and require megawatt proton sources, $1 - 3$ GeV neutrino beams and multi-kiloton detectors to make the observations. The measurements are further complicated by the low transition probability of $\nu_\mu \to \nu_e$ and the need to compare to $\overline{\nu}_\mu \to \overline{\nu}_e$ at high precision. This requires a detailed knowledge of the neutrino interaction cross-sections both for the dominant

signal processes and for background processes, such as $\nu N \to \nu N \pi^0$ where the π^0 is misidentified as an electron in a many kiloton sampling detector.

The phenomenology of neutrino cross-sections in relatively simple when $E\nu \ll 1$ GeV or when $E\nu \gg$ few GeV since these regimes are dominated by (quasi)-elastic and deep inelastic processes, respectively. However in the 1 to few GeV region, there are contributions to the cross-section from both of these processes as well as resonance-dominated hadroproduction. A successful phenomenological approach to modeling the resonance region in electron scattering is the use of quark-hadron duality to relate quark-model cross-sections to the cross-section over the discrete resonances [15] as shown in Fig. 9, Fig. 10 and Fig. 11. Figure 9 shows a fit by Bodek and Yang to inelastic electron and muon scattering data with a modified scaling variable and GRV98 PDFs with additional corrections (based on consideration of the Adler and Gilman sum rules [24]. Figure 10 and Figure 11 compare the predictions of the fit to data in the resonance region (which is not included in the fit, as well as other data such a photoproduction and high energy neutrino data). All predictions assume quark-model relations, and an empirical fit to R (R_{1998}). This approach requires the separation of the F_2, which has a simple representation in the quark model, and R whose description requires a different prescription. We hope to build successful models of neutrino scattering using this same prescription with the addition of a quark-model representation of the axial vector component of the cross-section. As mentioned earlier, since neutrino data are measured in nuclear targets, even in the quark model case, the separated vector structure functions from electron scattering, F_{2p}, F_{2n}, R_p, R_n for bound nucleons are needed in order to understand the axial structure function in neutrino scattering experiments.

The new precise data will also allow us to redo a combined analysis of electron-nucleon and neutrino nucleon data in the resonance region within the Feynman quark-oscillator model as done years ago (with poor precision) by Rein and Seghal [16], or use more sophisticated recent models (e.g. Sato and Lee [30]. In addition, there is on-going theoretical efforts to include nuclear effects (e.g. the Ghent group in Belgium [31] and the work of Paschos and Sakuda [32]. The results of the updated analysis within a resonance model can be compared to an analysis which is based on duality.

The full program of studies requires first additional precise electron scattering data, in particular σ_L and σ_T (or equivalently F_2 and R) on nuclear targets (materials suited for future neutrino oscillation detectors – water [17], hydrocarbons [3], liquid argon – and steel, where the most precise high energy neutrino cross-sections have been measured [18]) in the relevant kinematic regime. Later, as the new generation of high rate neutrino beams at Fermilab and J-PARC become available, the approach can be directly validated with comparisons to data from high rate neutrino cross-section experiments on the same targets [2].

With enough data to form a comprehensive modeling of electron-nucleon/nucleus and neutrino-nucleon/nucleus interactions, various sum-rules can then be tested. For example, the Adler [24] sum rules which are based on current algebra, are expected to be valid over the entire range in Q^2 and are expected to be exact. Other sum rules (mentioned earlier), which have QCD corrections, can be compared with expectations from QCD.
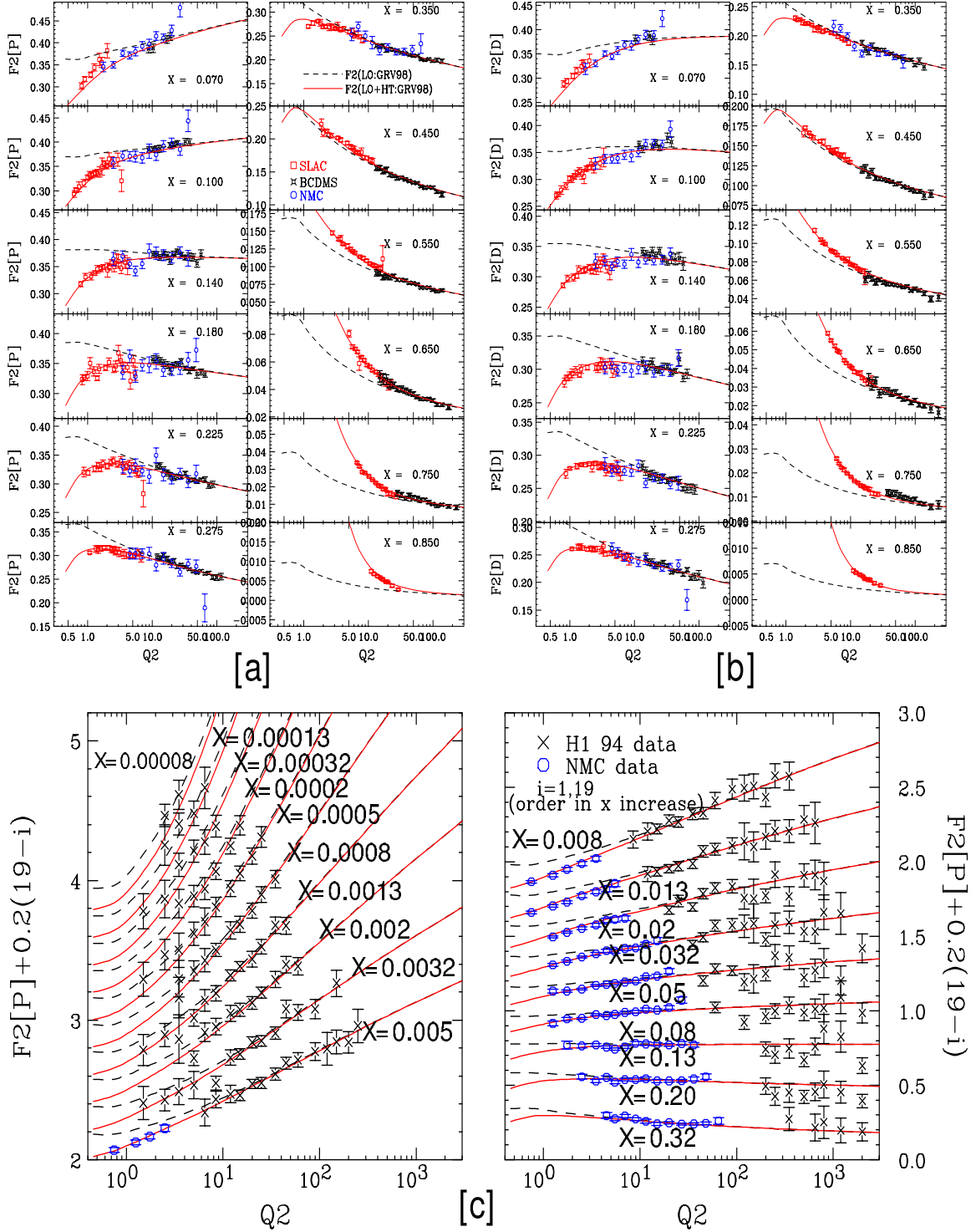
FIG. 9. Electron and muon F_2 data (SLAC, BCDMS, NMC, H1 94) used to obtain the parameters of the Bodek-Yang modified GRV98 ξ_w fit compared to the predictions of the unmodified GRV98 PDFs (LO, dashed line) and the modified GRV98 PDFs fits (LO+HT, solid line); [a] for F_2 proton, [b] for F_2 deuteron, and [c] for the H1 and NMC proton data at low x.

15
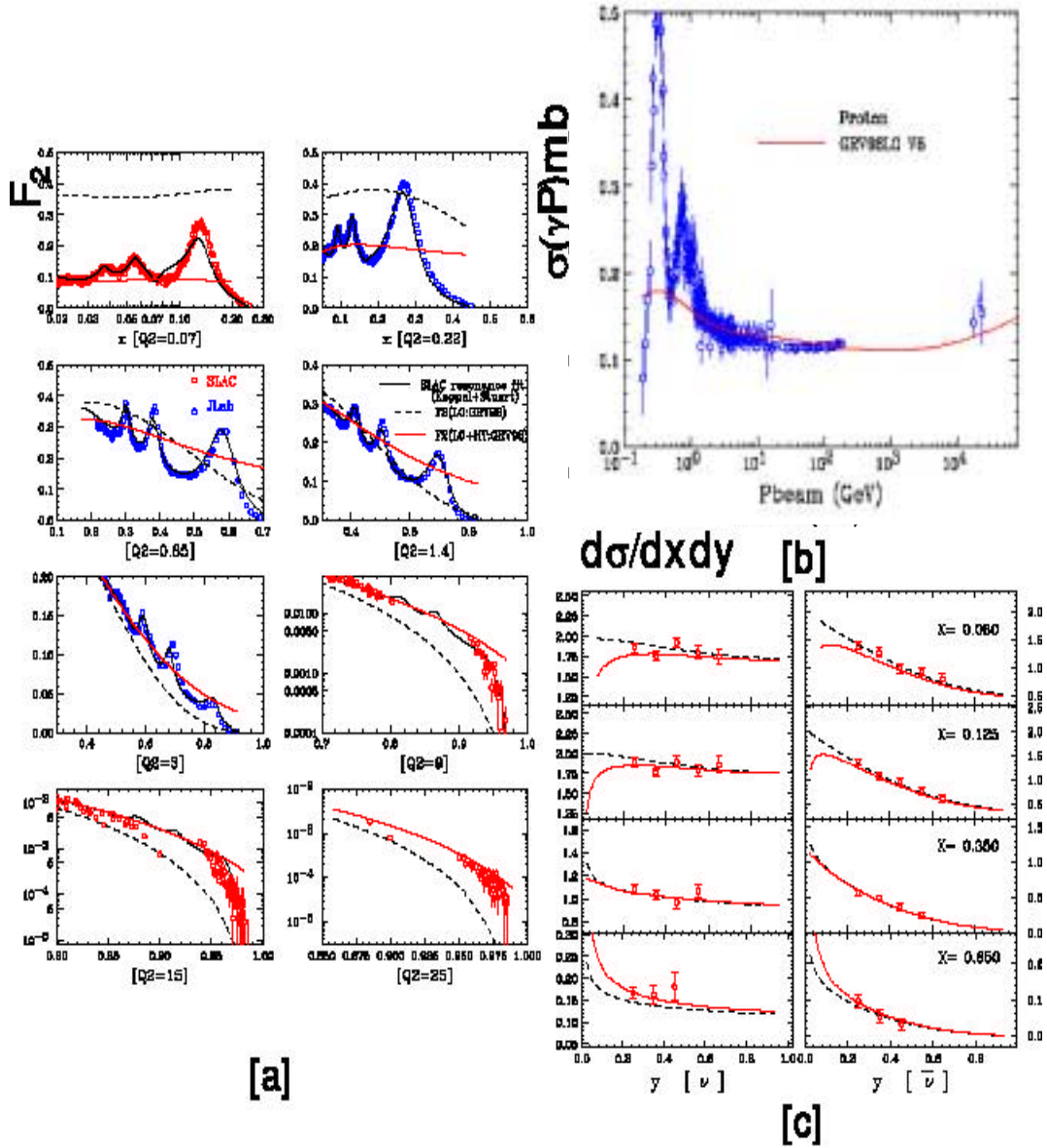
FIG. 10. Comparisons to proton and iron data not included in the Bodek-Yang GRV98 ξ_w fit. (a) Comparison of SLAC and JLab (electron) F_{2p} data in the resonance region (or fits to these data) and the predictions of the GRV98 PDFs with (LO+HT, solid) and without (LO, dashed) the Bodek-Yang modifications. (b) Comparison of photoproduction data on protons to predictions using Bodek-Yang modified GRV98 PDFs. (c) Comparison of representative CCFR ν_μ and $\overline{\nu}_\mu$ charged-current differential cross sections on iron at 55 GeV and the predictions of the GRV98 PDFs with (LO+HT, solid) and without (LO, dashed) Bodek-Yang modifications.
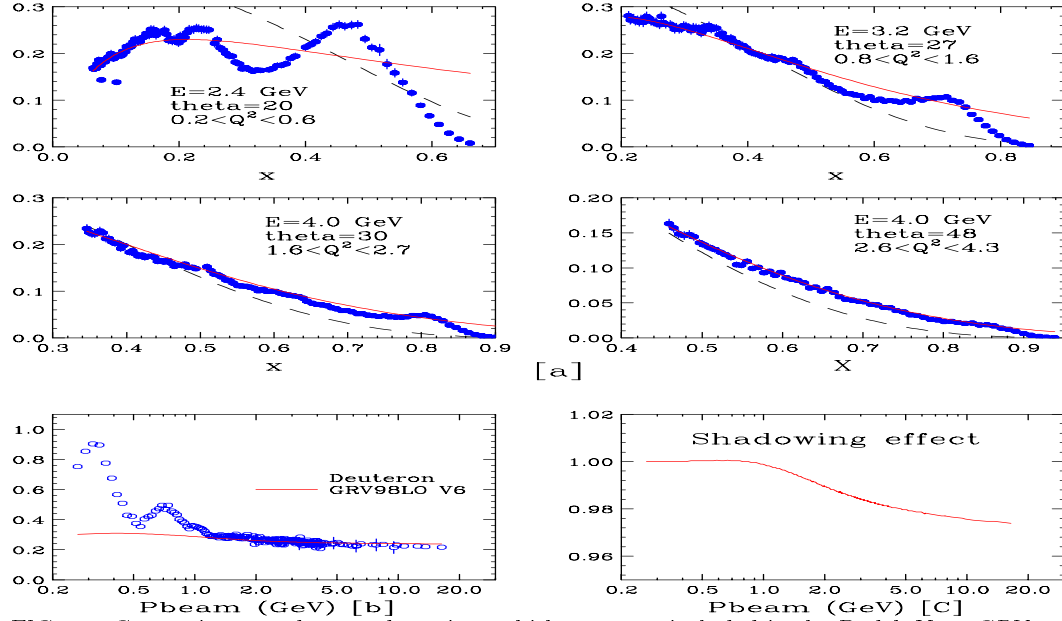
FIG. 11. Comparisons to data on deuterium which were not included in the Bodek-Yang GRV98 ξ_w fit. (a) Comparison of SLAC and JLab (electron) F_{2d} data in the resonance region and the predictions of the GRV98 PDFs with (LO+HT, solid) and without (LO, dashed) our modifications. (b) Comparison of photoproduction data on deuterium to predictions using Bodek-Yang modified GRV98 PDFs (including shadowing corrections). (c) The shadowing corrections that were applied to the PDFs for predicting the photoproduction cross section on deuterium.

$Target$	$(Z, A), Z/A$	$r.l.(g/cm^2)$	$r.l.(cm)$
H	(1, 1.00794), 0.99212	61.28	866
D	(1, 2.01404), 0.49652	122.4	724
C (approx CH2)	(6, 12.011), 0.49954	42.7	18.8
Ne	(10, 20.1797), 0.49555	28.94	14.0
Poly-CH2	0.53768	43.72	43.4
Water-H2O	0.55509	36.08	36.1
Quartz-SiO2	0.49926	27.05	12.3
O2(in Water, Quartz)	(8, 15.999), 0.50002		
Si(in Quartz)	(14, 28.0855), 0.49848	21.82	9.36
Al(Approx Si)	(13, 26.9815), 0.48181	24.01	8.90
Ar	(18, 39.948), 0.45059	19.55	14.0
Ca (approx Ar)	(20, 40.078), 0.49903	16.14	10.42
Fe	(26, 55.805), 0.46556	13.84	1.76
Cu (approx Fe)	(29, 63.506), 0.45636	12.86	1.43

TABLE I. Targets used in low energy low statistics neutrino experiments (H, D, Ne, Ar, Polystyrene Scintillator, Water, Iron), and additional targets that may be used to approximate them (Carbon, Quartz, Silicon, Calcium, Copper). Note that future high statistics experiments are planned with Hydrocarbon, Water and Iron targets.

17

NUCLEAR TARGETS AND KINEMATICS

Table II shows nuclear targets that we propose to add to the target ladder of experiment E02-109

Table I shows the kinds of nuclear targets that are of interest to neutrino experiments. which already is approved to take data with a Deuterium target and with an Aluminum empty target replica.

The differential cross sections for inclusive electron scattering on Deuterium will be measured in E02-109 according to the following definition:

$$\frac{d^2\sigma}{d\Omega dW^2} = \frac{\Delta N}{\Delta\Omega\Delta W^2}\frac{1}{Qnd},\qquad(9)$$

where ΔN is the counts per W^2 bin, n is the density of deuterium, d the target thickness, and Q is the integrated number of incident electrons on target. Table III gives a breakdown of beam time requirements for E02-109 for the Δ running only. The last column shows additional time that is needed to measure nuclear targets with the same number of events at each point as for Deuterium if this experiment (P03-110) were to run at the same time as E02-109.

$Target-Thickness\ r.l.$	$Running\ Ratio$	$Data$	$comment$
$H-0.005$	2.0	$All\ Q^2$	$Taken\ in\ E94-110$
$D-0.005$	1.0	$All\ Q^2$	$planned\ by\ E02-109$
$Al-0.005$	$(5.1*)$	$All\ Q^2$	$planned\ by\ E02-109$
$C-0.06$	0.2	$All\ Q^2$	$nominal$
$Quartz-0.06$	0.4	$Q^2<4$	$nominal$
$Si-0.06$	0.5	$Q^2<4$	$nominal$
$Ca-0.06$	0.6	$Q^2<4$	$nominal$
$Fe-0.06$	0.7	$Q^2<4$	$nominal$
$Cu-0.06$	0.8	$All\ Q^2$	$nominal$
$C-0.02$	0.7	$All\ Q^2$	$Rad-Cor$
$C-0.12$	0.1	$All\ Q^2$	$Rad-Cor$
$Cu-0.02$	2.4	$All\ Q^2$	$Rad-Cor$
$Cu-0.12$	0.4	$All\ Q^2$	$Rad-Cor$
$Fe-0.02$	2.2	$Q^2<4$	$Rad-Cor$
$Fe-0.12$	0.4	$Q^2<4$	$Rad-Cor$
$Water-0.02$	0.8	$Q^2<4$	$notused$

TABLE II. Targets to be used in this proposal (). Running Ratio is the ratio of the running time relative to running with a 4 cm (0.005 r.l.) Deuterium target to get the same number of events (at constant current of 80 μA, which is planned for E02-109). Note that data with Hydrogen is already available from JLab experiment E94-110, and Deuterium and Aluminum data need need NOT be taken if this experiment () runs at the same time as E02-109 (thus minimizing the error on the ratio of structure functions on nuclear targets to deuterium). All Q^2 identifies targets for which data will be taken at all values of Q^2, and $Q^2<4$ identifies targets for which no high Q^2 data will be taken. The nominal targets are identified. Rad-Cor indicates targets to be used for Radiative Corrections Studies, and TBI indicates Option To Be Investigated. $*$ Note that the Al target is only used for empty target, and therefore statistics equal to D2 are not needed.

A. Details of Event Rate Calculations

A minimum time of one half hour per kinematic setting, a maximum rate of 1000 Hz, and a beam current of 80 μA were used in the calculation of the running time for Deuterium for E02-109. The calculated rates listed are for bins of width $\Delta W^2 = (25\text{MeV})^2$ averaged over a momentum acceptance of $\pm 8\%$ and assuming an effective solid angle of the HMS of 6.5 msr at the Δ resonance. The data for the higher resonances comes in at higher rates and requires $\approx 50\%$ additional beam time. The data acquisition time listed in Table III reflects the total time required for the Δ resonance only. The SOS will be used to collect positron yields (from neutral pion production) for charge symmetric background studies and will be run in a simultaneous single arm mode with the HMS data and, so, this adds little time to the beam time request. The extraction of neutron structure functions from D_2 data for E02-109 requires the subtraction of the proton data taken in E94-110. As a cross check on relative normalizations, E02-109 plans to do measurements of the hydrogen resonance region cross sections for $Q^2 < 3.0$ $(\text{GeV/c}^2)^2$ to compare to E94-110. This takes an additional 8 hrs. A minimum central spectrometer momentum setting of 400 MeV/c was assumed. All proposed measurements with deuterium in E02-109 use the Hall C 4 cm deuterium target. In addition, E02-109 plans to take elastic proton data at all angles and energies for kinematic uncertainty checks.

Q^2_Δ $(GeV/c)^2$	E (GeV)	E'_Δ (GeV)	θ_Δ (deg)	ϵ_Δ	$Rate_\Delta$ (Hz)	D_2-Time (Hours) E02-109	Nucl. Tgts (hours) P03-110
0.5	1.16	0.55	52*	0.54	1 K	0.5	
	1.64	1.0	33	0.78	1 K	0.5	
	4.04	3.4	11	0.97	1 K	0.5	
1.0	1.64	0.77	52*	0.53	1 K	0.5	
	2.28	1.4	33	0.77	1 K	0.5	
	4.52	3.6	14	0.95	1 K	0.5	
2.0	2.28	0.87	60*	0.43	65	0.5	
	3.24	1.8	35	0.73	285	0.5	
	5.64	4.2	17	0.92	1 K	0.5	
3.0	3.24	1.3	52*	0.51	16	2	
	4.04	2.1	35*	0.70	40	1	
	5.64	3.7	22	0.86	172	0.5	
					sub-total	8	24
4.0	3.24	0.77	79*	0.23	1	22	
	4.04	1.6	47*	0.51	3	8	
	5.64	3.2	27	0.77	53	1	
5.0	4.04	1.0	66*	0.29	1	22	
	4.52	1.4	52*	0.42	3	8	
	5.64	2.5	35	0.66	6	4	
					sub-total	65	40
						Total D **73** E02-109	Total-Nucl **64** P03-110

TABLE III. D_2 Running for E02-109 Beam time requirements for all proposed measurements, as in the E02-109 proposal. All kinematics and rates shown are for a single bin in W^2 of 25 $(\text{MeV})^2$ width at the Δ resonance. Positron data will be taken in the SOS for the angles indicated by an asterisk. The last column is the additional time needed for heavy targets for this proposal: 6 targets at (C, Quartz, Si, Ca, Fe and Cu) $Q^2 < 4$ and 2 targets (C and Cu) at all Q^2. The beam energies in this table differ slightly and inconsequentially from those in this proposal text, as the original E02-109 energies were slightly disparate from the actual common JLab energies. The text energies are the correct ones for both experiments.

Note that the assumption made in the calculation of the rates for E02-109 are conservative. The 80 μA current is assumed to minimize density difference in the deuterium target. For some of the solid targets in the proposed experiment (P03-110) a higher current of 100 μA can be used (especially at high Q^2). Similarly, a data taking rate of 1000 Hz is also conservative and data can be taken with 2000 Hz (and possibly at 3000 Hz with some upgrades).

The chosen beam energies in the table assume a linac energy of 1.12 GeV (1.18, 2.30, 3,42, 4.54, 5.66), with the exception of two beam energies which assume a linac energy of 0.80 GeV (1.64, 4.04). Both base energies are standard CEBAF accelerator tunes. The required beam time was determined such that the statistical accuracy per W^2 bin was $\approx$ 3 times greater than the systematic point-to-point accuracy expected. The rates were estimated based upon a fit of previous deuterium resonance region cross section data from JLab [19]. Using the parameters in Table II we can scale the running time for Deuterium and obtain the corresponding additional running time for the nuclear targets (shown in the last columns of Table III and Table IV. The total beam time requested for both E02-109 (D_2) and for this experiment P03-110 (last column Nucl. Tgts) are listed in Table IV).

For D_2 running for E02-109 the total data acquisition time listed reflects the total time from Table III, as well as an additional 40 hours to complete the higher resonances, an additional 60 hours for dummy runs which are needed to subtract the yield contributions from the aluminum end caps of the target, an additional 24 hours needed to complete the hydrogen elastic scattering measurements, and an additional 16 hours to obtain hydrogen resonance region data which is needed for cross checks with E94-110. Also, since the positron data comes in at a slower rate, E02-109 requested an additional 22 hours to complete these measurements. The E02-109 proposal assumes one-quarter hour for each angle change required at a given beam energy, and one-quarter hour for each spectrometer central momentum change not possible to be done concurrently with angle changes. Combined with one day for checkout, the total beam time approved for E02-109 is 13 days [22].

This experiment (P03-110) requests an additional 5 days of running to do the measurements with the nuclear targets. With 2.5 days of additional running, data with all six targets can be measured for all of the E02-109 data points with $Q^2 < 4$. The additional 2.5 days are requested for the measurements at the higher Q^2.

	D- Time Required (Hours) E02-109	Nucl. Tgts. (Hours) P03-110
Data acquisition (Deuterium Δ)/+Nucl. Tgts.	73	64
Data acquisition (Deuterium $W^2 > \Delta$)/+Nucl. Tgts.	40	38
Data acquisition (Dummy)	60	
Data acquisition (hydrogen elastics)	24	
Data acquisition (hydrogen resonance region)	16	
Data acquisition (additional positrons)	22	
D Angle changes (12)/+Nucl. Tgt Changes	3	10
Spectrometer momentum changes (60)	15	
Major beam energy changes (1)	8	
Minor beam energy changes (5)	20	
D Checkout /+ Nucl. Rad correction Tests	24	10
Total	**305** E02-109	**120** P03-110

TABLE IV. D_2 Running for E02-109: Breakdown and tabulation of the total time requested. Based on previous experience, we assume one-half hour for angle changes, 15 minutes for momentum changes, eight hours for linac energy changes (major), and four hours for each energy change accomplished by changing the number of cycles (minor). The last column is the additional time required for heavy targets in this proposal (P03-110)

VII. THE COLLABORATION

The collaboration consists primarily of members of the current E02-109 collaboration, with the addition of collaborators from the MINERvA, NuTeV and MINOS Neutrino Experiments at Fermilab. These scientists have participated in a substantial amount of Hall C running. The collaboration has implemented and proven successful techniques to reduce systematical uncertainties in Hall C experiments, including detailed studies of spectrometer optics, spectrometer survey studies, raster phase analysis, and additional beam line instrumentation. This collaboration has the on-site experience, knowledge and expertise requisite to perform a precision measurement of the type proposed. These experimenters include spokespersons of the previous JLab experiments on which this proposal is founded (E94-110, E02-109 and E99-118).

This proposal brings a significant number of new collaborators from the University of Rochester and University of Massachusetts, including the two spokespersons of SLAC experiment E140 and E140X (Bodek and Rock), the Rochester NuTeV neutrino group, and the Rochester Nuclear Physics group (Manly). A significant portion of the collaboration plans to continue these studies with the MINERvA neutrino experiment at Fermilab (Rochester, Hampton, Jlab, and Tufts), including two of the Spokespersons of MINERvA (Keppel and McFarland).

Steve Manly (Rochester) and Will Brooks (Jlab) will also be looking at existing Hall B CLAS data at Jefferson Laboratory to study hadronic final states in electron scattering on nuclear targets (e.g. Carbon), and in particular final state in the quasielastic and resonance regions.

Two potential Rochester Ph.D. students are shown as well as Rochester theorists who have expressed interest in the results.

We are also in close contact with The Ghent (Jan Ryckebusch [31] nuclear theory group in Belgium, and the Argonne nuclear theory group (H. Lee [30] who are developing models that are applicable to both electron and neutrino reactions on d nuclei and nucleons. We plan to use these theoretical tools to do a combined analysis of the inclusive data from this experiment (P03-110) on Cargon, the Hall B data exclusive electron scattering data on Carbon, and the MINERvA neutrino data on Carbon. In addition, there are other theoretical efforts (e.g. Sakuda and Paschos) on nuclear effects for the hadronic final states in the region of the first resonance.

VIII. CONCLUSION

Using the existing Hall C apparatus, JLab experiment E02-109 has been approved to perform a global survey of L-T separated unpolarized structure functions on deuterium throughout the nucleon resonance region with an order of magnitude better precision than has been achieved before. The recent analysis of the proton data from E94-110 clearly show that these goals are both realistic and attainable. Furthermore, the analysis machinery previously developed can be used nearly without modification and should allow the analysis of the data to proceed in an accelerated fashion.

Here we propose another experiment (P03-110) that in only five days of additional running yields a substantial amount of new data with nuclear targets. These data are a key ingredient in a new program linking the nuclear and high-energy physics communities in investigating quark-hadron duality in nuclear targets using both electron and neutrino beams.

An immediate impact of these new measurements with nuclear targets will be the reduction in uncertainties in neutrino oscillation parameters for current and near term neutrino oscillations experiments such as K2K and MINOS. The data are even more important for the more precise next generation neutrino oscillations experiments such as JPARC and NUMI Off-axis.

APPENDIX A - RADIATIVE CORRECTIONS STUDIES

Thick Radiator Effects

SLAC-E140 [6] and SLAC-E139 [20] have performed tests with 0.02, 0.06 and 0.12 radiation length targets. Figure 12 illustrates that the radiative corrections can be well understood even for these relatively thick targets using the analysis techniques of E140. In this experiment, we add a variety of target thicknesses to repeat these radiative corrections tests in the JLab kinematic region.

In addition, in order to obtain more statistics with Aluminum in E01-109 (using the Aluminum Empty Target runs), we plan to go back to using thick empty targets, a technique pioneered at SLAC by Bodek [21]. The Aluminum Empty Target replica is made thicker to match the radiation length of the 0.005 r.l. Deuterium target. This greatly increases the counting rate for the empty target replica, as well as making sure that the radiative corrections for the empty target are indeed the same as the correction for the full Deuterium target. Therefore, if this target is used instead, then the 60 hours allocated for empty target replica by E02-109 can yield Aluminum data with about 1/6 of the statistics of the running with deuterium.
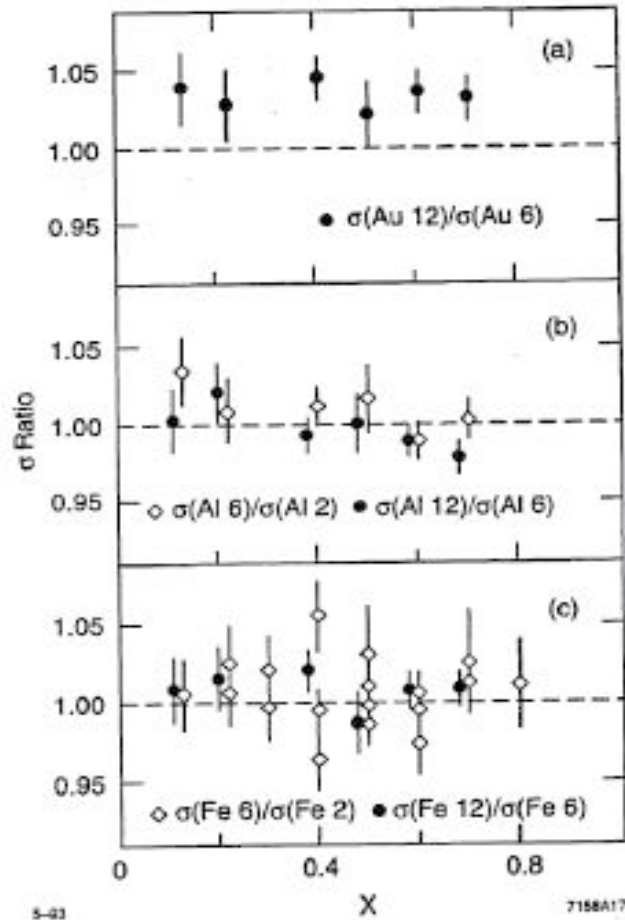

Fig. 26

FIG. 12. Radiative Corrections tests from SLAC E140 and E139.

Two Photon Effects

Recently, it has been suggested that the electric form factor of the proton as measured in electron scattering using the standard Rosenbluth separation technique [25], is sensitive to two-photon radiative corrections. This has been proposed to explain a difference between the Rosenbluth results and the results using the newer polarization transfer technique [26]. The polarization measurements do not directly measure the form factors, but measure the ratio G_E/G_M, as as shown in Figure 13.

For elastic scattering the ratio R is related to the ratio of form factors by the following expression $R_{elastic} = (4M^2/Q^2)(G_E/G_M)^2$, or $R^p_{elastic} = (0.481/Q^2)(\mu_p G^p_E/G^p_M)^2$. For the mean Q^2 of this experiment of 2.5 Gev^2 the data in figure 13 show that $R^p_{elastic}= (0.19)(0.88)^2$=0.14±0.04 from the fit to the Rosenbluth separation data and $R^p_e lastic$= $(0.192)(0.72)^2$=0.10±0.02 from the fit to the polarization transfer data. If this difference is to be attributed to two-photon effects, then it implies a 4% epsilon dependence in the radiative corrections and an uncertainty in R of 0.04 ± 0.02. *The uncertainty from two-photon effects in the inelastic radiative corrections is actually lower than this estimate because modern radiative corrections programs for inelastic electron and neutrino scattering (e.g. Bardin) already include two photon effects at the parton level.*
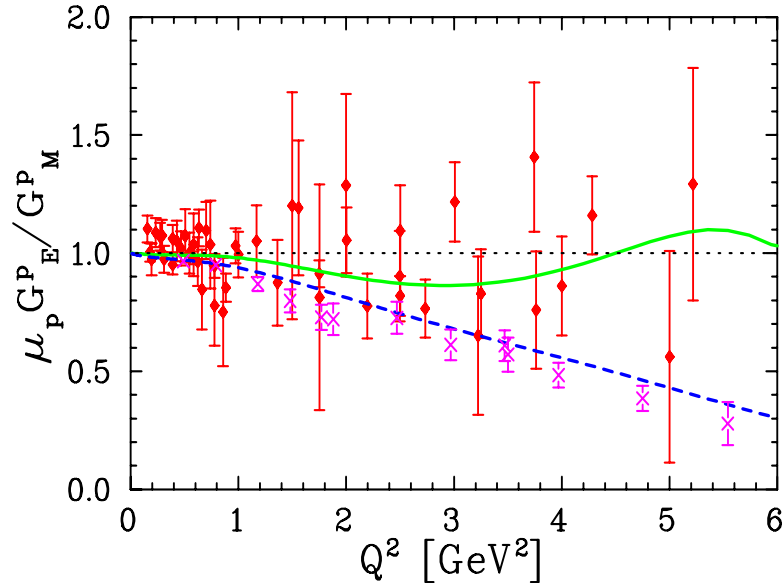

FIG. 13. Ratio $\mu_p G^p_E/G^p_M$ as extracted by Rosenbluth separation measurements (diamonds) and as obtained by polarization measurements(X's).

APPENDIX B - PRACTICAL ISSUES IN CHOICES OF TARGETS

A consideration in the choice of targets is the maximum amount of current that can be delivered without damaging or changing the density of the target. This experiment as proposed can be done in 5 days using standard targets, but we have made some compromises and may wish to consider future alternatives, as outlined below.

At present 0.02, 0.06 and 0.12 r.l. C, Fe and Cu targets already exist in Hall C. The current that the Fe target can withstand depends on the thermal contact with the water cooled frame. Safe current limits will likely be in a range 30–60μA, depending on the our confidence in this

thermal contact. In contrast, C and Cu can easily withstand 80 μA, and therefore those targets were chosen for the high Q^2 running.

The best measurement of cross-sections on water would come from use of the Hall A "waterfall" target, which consists of three "free-falling" water curtains, each of 250 mg/cm^2 and can probably withstand 100 μA. Issues to be investigated with this target include density variation with current and whether it is practical to add this target to the Hall C scattering chamber. Therefore, this kind of target is not part of the proposed run plan, but is a subject of investigation.

The existing Hall C Calcium target may have a current limitation of 30 μA. We plan to investigate if a new Calcium sandwich target may be able to handle higher current.

APPENDIX C -OTHER ELECTRON DATA THAT WILL BE USED IN OUR ANALYSIS

In addition to E94-110 (Hydrogen) and E02-103 (Deuterium), we also plan to use previous low Q^2 data in the inelastic region (e.g. Jlab experiment [7] E99-118), previous data from experiment E02-109 taken in the quasielastic region [23] (for radiative corrections), and also high Q^2 data from experiment E02-103 (hydrogen and deuterium quasielastic and resonance F_2 data) approved by Jlab PAC24 to run in 2004 (J. Arrington, spokesperson). Other lower precision high Q^2 data such as SLAC experiment E140 and E140x on nuclear targets will also be included in the overall analysis.

APPENDIX D: CHARGED-CURRENT NEUTRINO AND ANTINEUTRINO CROSS SECTIONS

Quark-Parton Model

Here we use the quark-parton model to illustrate some of physics concepts behind the proposed measurements. Note that at low energies, there are large corrections to this model which need to be taken into account.

In neutrino (ν_μ) nucleon scattering experiments, the three independently measured variables in a charged-current event are the outgoing muon momentum (p_μ), the outgoing muon angle (θ_μ), and the observed energy of the final state hadrons (E_{had}). From these measured variables the neutrino energy is equal to $E_\nu = E_{had} + E_\mu$ as required by energy conservation.

The derivation of the formulae for inclusive charged-current neutrino scattering is very similar to the case of $e - \mu$ scattering. Both do not require any knowledge of the dynamics inside the nucleon. The unknown couplings of the lepton-current to the nucleon are absorbed in the definition of the structure function F_i. In the case of elastic (muon,electron) or quasi-elastic (neutrino) scattering, these can be interpreted as the Fourier transforms of the spacial charge distribution in the nucleon.

The general form of the differential cross section for neutrino-nucleon scattering, mediated by the W boson (in the case of charged-current scattering) is given in terms of three structure functions:

$$\frac{d^2\sigma^{\nu(\overline{\nu})}}{dxdy} = \frac{G^2ME}{\pi}\left[(1 - y - \frac{Mxy}{2E})F_2 + \frac{y^2}{2}2xF_1 \pm (1 - \frac{y}{2})xF_3\right] \tag{10}$$

where the $+(-)$ terms correspond to neutrino (antineutrino) scattering. Here G_F is the Fermi weak coupling constant. The structure function, F_i are process dependent, and are functions of the kinematics variable, x and Q^2. If the cross section is re-written in terms of the absorption cross-sections by left-handed, right-handed, and longitudinally polarized W bosons, then the structure function F_1 corresponds to the contribution from the sum of left-handed and right-handed bosons, F_2 corresponds to the contribution from all boson polarizations, whereas F_3 corresponds to the contribution from the difference of right-handed and left-handed polarized

bosons. The structure function F_3 is non-zero only in weak interactions (for which parity is violated).

The relationship between the experimentally extracted structure functions and the parton distributions in the nucleon (and their dependence on kinematic variables) is determined within the framework of the quark-parton model. If we denote $q(x)$ as the probability to find a parton with momentum fraction x in a frame of a fast moving nucleon, the differential cross section for the scattering from a parton is given by

$$\frac{d\sigma^2}{dx\,dy} \propto \frac{G_F^2 M E}{\pi(1+Q^2/M_W^2)^2}\, x\,q(x).$$ (11)

Therefore, the cross sections for neutrino (and antineutrino) nucleon scattering are the sums of all parton contributions in the nucleon, with the proper angular dependence factors, as follows:

$$\frac{d^2\sigma^{\nu N}}{dxdy} = \frac{G_F^2 M E_\nu x}{\pi(1+Q^2/M_W^2)^2}\left[q^{\nu N}(x) + (1-y)^2 \overline{q}^{\nu N}(x) + 2(1-y)k^{\nu N}(x)\right]$$ (12)

$$\frac{d^2\sigma^{\overline{\nu} N}}{dxdy} = \frac{G_F^2 M E_\nu x}{\pi(1+Q^2/M_W^2)^2}\left[\overline{q}^{\overline{\nu} N}(x) + (1-y)^2 q^{\overline{\nu} N}(x) + 2(1-y)k^{\overline{\nu} N}(x)\right]$$ (13)

The contribution (k) of the longitudinal contribution e.g. from possible spin-0 constituents or quark transverse momenta is also shown. The angular dependence factor for this contribution, $(1-y)$, is the same as for the terms which originate from the small intrinsic transverse (p_t) of spin 1/2 partons.

Total neutrino and antineutrino cross sections

Integrating the above expression over x and y (from 0 to 1) yields:

$$\sigma^{\nu N} = \frac{G_F^2 M E_\nu}{\pi(1+Q^2/M_W^2)^2}\left[Q^{\nu N} + (1/3)\overline{Q}^{\nu N} + K^{\nu N}\right]$$ (14)

$$\sigma^{\overline{\nu} N} = \frac{G_F^2 M E_\nu}{\pi(1+Q^2/M_W^2)^2}\left[\overline{Q}^{\overline{\nu} N} + (1/3)Q^{\overline{\nu} N} + K^{\overline{\nu} N}\right]$$ (15)

Here Q is the fractional momentum carried by all quarks in the nucleon, $\overline{Q}$ is the fractional momentum carried by all antiquarks in the nucleon and $R = 2K/(Q+\overline{Q})$ is the average ratio of longitudinal to transverse contribution. For low energies, the antiquark contribution is small. Therefore, the fractional error in the predicted neutrino and antineutrino total cross sections from an uncertainty in R is $0.5\Delta R$ for neutrinos and $1.5\Delta R$ for antineutrinos, respectively.

In the region of the first resonance, R is predicted to be zero in the bound quark oscillator model. In fact, the first results from Jlab experiment E94-110 on hydrogen (shown in Figure 7) show a value of R of about 0.3 at low W and low Q^2. This implies that the effects of the nucleon pion cloud are very important in this region. The nuclear dependence of R in the region is totally unknown, and current measurements of the nuclear dependence of R have an error of ΔR of 0.2. It is expected that the nuclear effects on the nucleon pion cloud are very significant at low energies. Therefore, even if we use the preliminary precise measurement of R on hydrogen from experiment E94-110, we are still left with the problem that none of the data have been taken on Carbon or iron. An error ΔR of 0.2 implies a 10% error in the predicted neutrino cross section in this region and an error 30% in the predicted antineutrino cross setion.

A back of an envelope calculation of the sensitivity of the ratio of antineutrino to neutrino total cross section ratio to a change in the average value of R with neutrino energy or from nuclear effects (e.g. $R = 0.3 \pm 0.2$) is illustrative. At low energy, with $\overline{Q}$=0 we obtain the following. If $R = 0$, the ratio is 0.33. If $R = 0.5$, the ratio is $(0.33 + 0.25)/(1.0 + 0.25)$=0.46. The data shown in Figure 1 span all of this range.

Structure Functions

A comparison of the above parton-level cross sections with Equation 10 yields the following relations between the structure functions and parton distributions:

$$2xF_1^{\nu(\overline{\nu})N} = 2\left[xq^{\nu(\overline{\nu})N}(x) + x\overline{q}^{\nu(\overline{\nu})N}(x)\right]$$

$$F_2^{\nu(\overline{\nu})N} = 2\left[xq^{\nu(\overline{\nu})N}(x) + x\overline{q}^{\nu(\overline{\nu})N}(x) + 2xk^{\nu(\overline{\nu})N}(x)\right] \tag{16}$$

$$xF_3^{\nu(\overline{\nu})N} = 2\left[xq^{\nu(\overline{\nu})N}(x) - x\overline{q}^{\nu(\overline{\nu})N}(x)\right] \tag{17}$$

where terms proportional to Q^2/ν^2 have been neglected. Thus, in the parton model, nucleon structure functions are related to the momentum distributions carried by the partons in the nucleon.

If the scattering takes place exclusively from free spin-$\frac{1}{2}$ constituents, the Callan-Gross relation

$$2xF_1 = F_2 \tag{18}$$

is satisfied. However, the partons also have non-negligible transverse momenta, which at present energies yields an apparent spin-0 type behavior, in the infinite momentum frame. This transverse momentum leads to a difference between F_2 and $2xF_1$ that diminishes as the momentum transfer Q^2 increases. The exact relation between $2xF_1$ and F_2 is obtained by using R, the ratio of the longitudinal structure function (F_L) and transverse structure function $(2xF_1)$.

$$R = \frac{F_L}{2xF_1} = \frac{F_2}{2xF_1}(1 + Q^2/\nu^2) - 1 = (1 + \frac{2k}{q + \overline{q}})(1 + Q^2/\nu^2) - 1. \tag{19}$$

Relation to Electromagnetic Structure Functions

The analogous expressions for charged-lepton scattering via virtual photon exchange follow from the pure vector nature of the electromagnetic current. Thus, electromagnetic scattering probes the charge of the partons, whereas neutrino scattering probes the flavor composition of the nucleon constituents.

$$2xF_1^{\ell N} = \sum_i e_i^2\left[xq_i^{\ell N}(x) + x\overline{q}_i^{\ell N}(x)\right] \tag{20}$$

$$F_2^{\ell N} = \sum_i e_i^2\left[xq_i^{\ell T}(x) + x\overline{q}_i^{\ell N} + 2k_i^{\ell N}(x)\right] \tag{21}$$

where e_i is electric charge of parton i. Comparison of neutrino and charged-lepton scattering data provides the measurement of the mean-square charge of the nucleon's interacting constituents.

Neutrino scattering has the ability to resolve the flavor of the nucleon constituents. Because of charge conservation at the quark vertex, charged current neutrino scattering happens only with d, s, $\overline{u}$ and $\overline{c}$ quarks. Similarly, antineutrinos can scatter only from $\overline{d}$, $\overline{s}$, u and c quarks. For a proton target, the parton densities that contribute to the structure functions are:

$$q^{\nu p}(x) = d^p(x) + s^p(x); \overline{q}^{\nu p}(x) = \overline{u}^p(x) + \overline{c}^p(x) \tag{22}$$

$$q^{\overline{\nu}p}(x) = u^p(x) + c^p(x); \overline{q}^{\overline{\nu}p}(x) = \overline{d}^p(x) + \overline{s}^p(x) \tag{23}$$

Isospin invariance (also called charge symmetry) requires symmetry between the light quark densities in the proton and neutron:

$$d^p(x) = u^n(x), \quad u^p(x) = d^n(x), \quad \overline{d}^p(x) = \overline{u}^n(x), \quad \overline{u}^p(x) = \overline{d}^n(x). \tag{24}$$

26

Using these symmetries, the quark distributions in the neutron are described in terms the quark distributions in the proton. All of the parton distributions are defined with respect to the proton.

$$q^{\nu n}(x) = u(x) + s(x); \overline{q}^{\nu n}(x) = \overline{d}(x) + \overline{c}(x) \tag{25}$$

$$q^{\overline{\nu} n}(x) = d(x) + c(x); \overline{q}^{\overline{\nu} n}(x) = \overline{u}(x) + \overline{s}(x) \tag{26}$$

Finally, the parton densities for an isoscalar nucleon, $\frac{1}{2}$(proton + neutron), are given by:

$$q^{\nu N}(x) = \frac{1}{2}\left[u(x) + d(x) + 2s(x)\right]; \overline{q}^{\nu N}(x) = \frac{1}{2}\left[\overline{u}(x) + \overline{d}(x) + 2\overline{c}(x)\right] \tag{27}$$

$$q^{\overline{\nu} N}(x) = \frac{1}{2}\left[u(x) + d(x) + 2c(x)\right]; \overline{q}^{\overline{\nu} N}(x) = \frac{1}{2}\left[\overline{u}(x) + \overline{d}(x) + 2\overline{s}(x)\right] \tag{28}$$

The quark content of the isoscalar structure function $2xF_1$ for neutrino scattering is obtained by substituting these densities into Equations 16:

$$\begin{aligned}
2xF_1^{\nu N}(x) &= xu(x) + x\overline{u}(x) + xd(x) + x\overline{d}(x) \\
&\quad + xs(x) + x\overline{s}(x) + xc(x) + x\overline{c}(x) \\
&= 2xF_1^{\overline{\nu} N}(x).
\end{aligned} \tag{29}$$

In the following discussion (for simplicity) we assume $xs(x) = x\overline{s}(x)$. The charm quark distributions, which are small when compared to the strange quark distributions, are also neglected.

The electromagnetic structure functions $2xF_1^{\ell p}$ and $2xF_1^{\ell n}$ are constructed from Equation 21 using the same parton densities as above, and including the quark charges:

$$\begin{aligned}
2xF_1^{\ell p} &= \left(\frac{1}{3}\right)^2 \left[xd(x) + x\overline{d}x + xs(x) + x\overline{s}(x)\right] \\
&\quad + \left(\frac{2}{3}\right)^2 \left[xu(x) + x\overline{u}(x) + xc(x) + x\overline{c}(x)\right]
\end{aligned} \tag{30}$$

$$\begin{aligned}
2xF_1^{\ell n} &= \left(\frac{1}{3}\right)^2 \left[xu(x) + x\overline{u}x + xs(x) + x\overline{s}(x)\right] \\
&\quad + \left(\frac{2}{3}\right)^2 \left[xd(x) + x\overline{d}(x) + xc(x) + x\overline{c}(x)\right].
\end{aligned} \tag{31}$$

$$\tag{32}$$

The $2xF_1^{\ell N}$ for an isoscalar nucleon is found by averaging:

$$\begin{aligned}
2xF_1^{\ell N} &= \frac{1}{2}\left(2xF_1^{\ell p} + 2xF_1^{\ell n}\right) \\
&= \frac{5}{18}\left(xu + x\overline{u} + xd + x\overline{d}\right) \\
&\quad + \frac{1}{9}\left(xs + x\overline{s}\right) + \frac{4}{9}\left(xc + x\overline{c}\right).
\end{aligned} \tag{33}$$

Under the assumption that the value of R is the same for electromagnetic neutral-current and weak charged-current structure functions, the ratio of electromagnetic and neutrino structure functions for $2xF_1$ is equal to the ratio for F_2:

$$\frac{F_2^{\ell N}}{F_2^{\nu N}} = \frac{5}{18}\left(1 - \frac{3}{5}\frac{xs + x\overline{s} - xc - x\overline{c}}{xq + x\overline{q}}\right) \tag{34}$$

where $xq + x\overline{q} = 2xF_1^{\nu N}$. This relationship is known as the $5/18ths$ rule. The observation that charged-lepton scattering and neutrino-scattering structure functions are approximately related by a factor of $\sim 5/18$, was a significant triumph for the QPM.

The structure function xF_3 (which is only present in parity violating weak interactions) represents the momentum density of valence quarks. Substitution of the isoscalar parton densities into Equation 17 yields:

$$xF_3^{\nu N}(x) = xu_V(x) + xd_V(x) + 2xs(x) - 2xc(x) \tag{35}$$

$$xF_3^{\overline{\nu} N}(x) = xu_V(x) + xd_V(x) - 2x\overline{s}(x) + 2x\overline{c}(x) \tag{36}$$

where $u_V \equiv u - \overline{u}$ and $d_V \equiv d - \overline{d}$ are the valence densities in the proton. The average value of $xF_3^{\nu N}$ and $xF_3^{\overline{\nu} N}$ yields the total valence quarks distribution. The difference of $xF_3^{\nu N}$ and $xF_3^{\overline{\nu} N}$ is very sensitive to both the strange sea and charm sea in the nucleon as shown below:

$$xF_3(x) = \left[xF_3^{\nu N}(x) + xF_3^{\overline{\nu} N}(x) \right] / 2 = xu_v(x) + xd_d(x) \tag{37}$$

$$\Delta xF_3(x) = \left[xF_3^{\nu N}(x) - xF_3^{\overline{\nu} N}(x) \right] = 2(s(x) + \overline{s}(x) - c(x) - \overline{c}(x)) \tag{38}$$

REFERENCES

[1] $http://www.pas.rochester.edu/bodek/jlab/F2 - Rnuclear - HallC.pdf$ A resubmission of P03-110

http://www.jlab.org/exp_prog/PACpage/PAC24/PACinfo.html

[2] Fermilab MINERvA NUMI Neutrino proposal $http://nuint.ps.uci.edu/files/$. The EOIs from the groups that combined to form the MINERvA collaboration, the NuMI On-axis and NuMI Off-axis groups, can be found on the MINERvA home page at: $http://www.pas.rochester.edu/minerva/$

[3] The NUMI Low Energy Neutrino Program at Fermilab.
http://www-numi.fnal.gov/fnal_minos/new_initiatives/new_initiatives.html

[4] JLab hydrogen experiment 94-110, C.E. Keppel spokesperson

(http://www.jlab.org/exp_prog/proposals/94/PR94-110.pdf)

[5] JLab deuterium experiment 02-109, C.E. Keppel, M. E. Christy, spokespersons

(http://www.jlab.org/exp_prog/proposals/02/PR02-109.ps)

[6] SLAC Experiment E140, A. Bodek and S. Rock, Spokespersons; S. Dasu et al., Phys. Rev. Lett. 61, 1061 (1988); S. Dasu et al., Phys. Rev. D49, 5641 (1994) ; S. Dasu, Ph.D. Thesis, University of Rochester, 1988 (UR-1059).

[7] JLab experiment 99-118 on the nuclear dependence of R in the DIS region at low Q^2, A. Brull, C.E. Keppel spokespersons

(http://www.jlab.org/exp_prog/proposals/99/PR99-118.pdf)

[8] M.N. Rosenbluth, Phys. Rev. 79, 615 (1956)

[9] Y. Fukada et al., Phys.Rev.Lett. 81 (1998) 1562.

[10] SNO Collaboration, nucl-ex/0204008, nucl-ex/0204009.

[11] K. Eguchi et al. [KamLAND Collaboration], Phys. Rev. Lett. **90**, 021802 (2003).

[12] A. Aguilar et al. [LSND Collaboration], anti-nu/e appearance in a anti-nu/mu beam," Phys. Rev. D **64**, 112007 (2001).

[13] M. Apollonio et al., Phys.Lett. **B466** (1999) 41.

[14] F. Boehm et al., Nucl.Phys.Proc.Suppl. 91 (2001).

[15] A. Bodek and U. K. Yang, `hep-ex/0203009`, Nucl.Phys.Proc.Suppl.112:70-76,2002.
A. Bodek and U. K. Yang, `hep-ex/0301036`.
A. Bodek, U. K. Yang, `hep-ex/0210024`, J. Phys. G. Nucl. Part. Phys.,**29**, 1 (2003). These were based on previous work by Bodek and Yang including studies in NLO +TM +HT (Phys. Rev. Lett 82, 2467 (1999) ; Phys. Rev. Lett. 84, 3456 (2000)) and studies in NNLO +TM +HT (Eur. Phys. J. C13, 241 (2000))

[16] D. Rein and L. M. Sehgal, Annals Phys. **133** 79 (1981) ;D. Rein, Z. Phys. C. 35, 43 (1987); R. P. Feynman, M. Kislinger and F. Ravndal, Phys. Rev. D**3**, 2706 (1971); and R. Belusevic and D. Rein, Phys. Rev. D **46**, 3747 (1992).

[17] Y. Itow *et al.*, "The JHF-Kamioka Neutrino Project", `hep-ex/0106019`.

[18] U. K. Yang *et al.*(CCFR), Phys. Rev. Lett. **87**, 251802 (2001).

[19] I. Niculescu. Ph.D. Thesis, Hampton University (1999)

[20] J. G. Gomez, Ph.D. Thesis, American University (1987). The 0.12 radiation length data is unpublished and it has only been used for tests of the external radiative corrections,

[21] A. Bodek, Nucl. Inst. Meth. 103, 603 (1973)

[22] `http://www.jlab.org/exp_prog/generated/hallc.html`

[23] JLab experiments in the quasielastic region (e.g. E02-109), from

(`http://www.jlab.org/exp_prog/generated/nucleon.html`)

[24] S. L. Adler, Phys. Rev.**143**, 1144 (166); F. Gilman, Phys. Rev. **167**, 1365 (1968).

[25] J. Arrington, nucl-ex/0305009.

[26] M. K. Jones *et al.*, Phys. Rev. Lett, 84, (2000) 1398 ; O. Gayou *et al.*, Phys. Rev. Lett, 88 (2002) 092301.

[27] International Workshops on Neutrino-Nucleus Interactions in the Few GeV Region: NUINT04(Grand Sasso): *http : //nuint04.lngs.infn.it/*; NUINT02 (Irvine): *http : //nuint.ps.uci.edu/*; NUINT01(KEK): *http : //neutrino.kek.jp/nuint0/*

[28] Arie Bodek, Conference Summary Talk, Proceedings of the Second International Workshop on Neutrino-Nucleus Interactions in the Few GeV Region: NUINT02 (Irvine): *http : //nuint.ps.uci.edu/*

[29] G.A. Miller, Phys.Rev. C 64,022201(2001) (REVEALING NUCLEAR PIONS USING ELECTRON SCATTERING. nucl-th/0104025)

[30] K. Sato and T. S. H. Lee nucl-th/0303050 (2003) (neutrino production); T. Sato, D. Uno and T.S. Lee, Phys. Rev. C63.-55201 (2001) (electroproduction)

[31] Ghent Theory group in Belgium (Jan Ryckebusch, jan@inwpent5.UGent.be)

(`http://inwpent5.ugent.be/papers/santorini.pdf`)

[32] E. A. Paschos, L. Pasquali and J. Y. Yu, Nucl. Phys. B 588, 263 (2000) and E. A. Paschos, J. Y. Yu and M. Sakuda [arXiv:hep-ph/0308130].